REPORT DOCUMENTATION PAGE

Form Approved OMB NO. 0704-0188

1. REPORT DATE (DD-MM-YYYY)	2. REPORT TYPE	3. DATES COVERED (From - To)
03-01-2011	Final Report	25-Sep-2003 - 30-May-2008

4. TITLE AND SUBTITLE
Agile Photonic Crystals

5a. CONTRACT NUMBER
DAAD19-03-1-0357

5b. GRANT NUMBER

5c. PROGRAM ELEMENT NUMBER
3D10M7

6. AUTHORS
Yoel Fink

5d. PROJECT NUMBER

5e. TASK NUMBER

5f. WORK UNIT NUMBER

7. PERFORMING ORGANIZATION NAMES AND ADDRESSES
Massachusetts Institute of Technology
Office of Sponsored Programs
Bldg. E19-750
Cambridge, MA 02139 -4307

8. PERFORMING ORGANIZATION REPORT NUMBER

9. SPONSORING/MONITORING AGENCY NAME(S) AND ADDRESS(ES)
U.S. Army Research Office
P.O. Box 12211
Research Triangle Park, NC 27709-2211

10. SPONSOR/MONITOR'S ACRONYM(S)
ARO

11. SPONSOR/MONITOR'S REPORT NUMBER(S)
45624-PH.1

12. DISTRIBUTION AVAILIBILITY STATEMENT
Approved for Public Release; Distribution Unlimited

13. SUPPLEMENTARY NOTES
The views, opinions and/or findings contained in this report are those of the author(s) and should not contrued as an official Department of the Army position, policy or decision, unless so designated by other documentation.

14. ABSTRACT
Abstract—We present an approach to the fabrication of functional fiber-based devices by thermal drawing in the viscous state termed the preform-to-fiber approach. A macroscopic preform rod containing metallic, semiconducting, and insulating constituents in a variety of geometries and close contact produces kilometer-long novel nanostructured fibers and fiber devices. A material identification scheme and the challenges of composite material processing are reviewed, and several devices and applications are discussed in detail.

15. SUBJECT TERMS
Fibers, multimaterial

16. SECURITY CLASSIFICATION OF:			17. LIMITATION OF ABSTRACT	15. NUMBER OF PAGES	19a. NAME OF RESPONSIBLE PERSON
a. REPORT	b. ABSTRACT	c. THIS PAGE			Yoel Fink
UU	UU	UU	UU		19b. TELEPHONE NUMBER 617-258-6113

Report Title

Agile Photonic Crystals

ABSTRACT

Abstract—We present an approach to the fabrication of functional fiber-based devices by thermal drawing in the viscous state termed the preform-to-fiber approach. A macroscopic preform rod containing metallic, semiconducting, and insulating constituents in a variety of geometries and close contact produces kilometer-long novel nanostructured fibers and fiber devices. A material identification scheme and the challenges of composite material processing are reviewed, and several devices and applications are discussed in detail. Metal-semiconductor-metal photosensitive and thermally-sensitive fibers are described. These flexible, light-weight, and low-cost functional fibers may pave the way for new types of fiber sensor devices, such as thermal sensing fabrics, artificial skins, and large-area optoelectronic screens. Next, the preform-to-fiber approach is used to fabricate spectrally tunable photodetectors that integrate a photosensitive core and a nanostructured photonic crystal defect cavity. An integrated self-monitoring optical transmission waveguide is then described that incorporates optical transport and thermal monitoring. The ability to predict power transmission failure is of paramount importance if high power optical transmission lines are to be operated safely and reliably in medical, industrial and defense applications. A hybrid electron-photon fiber consisting of hollow core (for optical transport by means of a photonic band gap) and metallic wires (for electron transport) is fabricated and may be used for transporting atoms and molecules by radiation pressure. Finally, a solid microstructured fiber fabricated with a highly nonlinear chalcogenide enables the generation of spectrally broadened light at near-infrared wavelengths.

List of papers submitted or published that acknowledge ARO support during this reporting period. List the papers, including journal references, in the following categories:

(a) Papers published in peer-reviewed journals (N/A for none)

Kuriki, K., Shapira, O., Hart, S., Benoit, G., Kuriki, Y., Viens, J.F., Bayindir, M., Joannopoulos, J.D., Fink, Y. “Hollow Multilayer Fibers for NIR Applications”, Optics Express 12, No. 8, 1510-1517, April 2004.

Bayindir, M., Sorin, F., Hart, S., Shapira, O., Joannopoulos, J.D., Fink, Y., “Metal-Insulator-Semiconductor Optoelectronic Fibres”, Nature 431, 826-829, October 2004.

Bayindir, M., Abouraddy, A.F., Sorin, F., Joannopoulos, J.D., Fink, Y., ”Fiber Photodetectors Codrawn from Conducting, Semiconducting and Insulating Materials”, OPN, Optics in 2004, 15, 12, 24, December 2004.

Benoit, G., Kuriki, K., Viens, J.F., “Dynamic All-Optical Tuning of Transverse Resonant Cavity Modes in Photonic Bandgap Fibers”, Optics Letters 30, 1620-1622, July 2005.

Bayindir, M., Shapira, O., Saygin-Hinczewski, D., Viens, J., Abouraddy, A.F., Joannopoulos, J.D., Fink, Y., “Integrated Fibers for Self Monitored Optical Transport”, Nature Materials 4, No. 11, 820-825, November 2005.

Abouraddy, A.F., Shapira, O., Bayindir, M., Arnold, J., Sorin, F., Saygin-Hinczewski, D., Joannopoulos, J.D., Fink, Y., "Large-Scale Optical-Field Measurements with Geometric Fibre Constructs", Nature Materials 5, No. 7, 532-536, July 2006.

Number of Papers published in peer-reviewed journals: 6.00

(b) Papers published in non-peer-reviewed journals or in conference proceedings (N/A for none)

Number of Papers published in non peer-reviewed journals: 0.00

(c) Presentations

March 2005, “Metal Insulator Semiconductor Mesostructured Fibers”, Ecole Polytechnique, Montreal, Canada.

April 2005, “Metal Insulator Semiconductor Mesostructured Fibers”, NPIS, San Diego, CA.

June 2005, “Metal Insulator Semiconductor Mesostructured Fibers”, International Conference on Electroceramics, Seoul, Korea (plenary talk).

June 2005, “Multimaterial Photonic Bandgap Mesostructured Fiber”, Weizmann Institute, Israel.

July 2005, “Metal-Insulator-Semiconductor Fibers: Spanning the Nano to Macro Divide”, Gordon Research Conference on Clusters, Nanocrystals and Nanostructures, Connecticut.

October 2005, “Metal-Insulator-Semiconductor Optoelectronic Fiber Sensors”, Optics East 2005, Boston.

Number of Presentations: 6.00

Non Peer-Reviewed Conference Proceeding publications (other than abstracts):

Number of Non Peer-Reviewed Conference Proceeding publications (other than abstracts): 0

Peer-Reviewed Conference Proceeding publications (other than abstracts):

Number of Peer-Reviewed Conference Proceeding publications (other than abstracts): 0

(d) Manuscripts

Number of Manuscripts: 0.00

Patents Submitted

M. Bayindir, F. Sorin, A.F. Abouraddy, O. Shapira, J. Arnold, Y. Fink, J.D. Joannopoulos, “Thermal sensing fiber devices”, US Patent No. 7,567,740, July 28, 2009.

M. Bayindir, F. Sorin, A.F. Abouraddy, O. Shapira, J. Arnold, Y. Fink, J.D. Joannopoulos, “Thermal sensing fiber devices”, US Patent No. 7,567,740, July 28, 2009.

Patents Awarded

M. Bayindir, F. Sorin, D. S. Hinczewski, S. Hart, “Optoelectronic fiber codrawn from conducting, semiconducting, and insulating materials”, US Patent No. 7295734, November 13, 2007.

M. Bayindir, F. Sorin, A.F. Abouraddy, O. Shapira, J. Arnold, Y. Fink, J.D. Joannopoulos, “Thermal sensing fiber devices”, US Patent No. 7,567,740, July 28, 2009.

Awards

None.

Graduate Students

NAME	PERCENT SUPPORTED
Fabien Sorin	1.00
Ofer Shapira	1.00
Shandon D. Hart	1.00
Gilles Benoit	1.00
FTE Equivalent:	**4.00**
Total Number:	**4**

Names of Post Doctorates

NAME	PERCENT SUPPORTED
Mehmet Bayindir	1.00
FTE Equivalent:	**1.00**
Total Number:	**1**

Names of Faculty Supported

NAME	PERCENT SUPPORTED
FTE Equivalent:	
Total Number:	

Names of Under Graduate students supported

NAME	PERCENT SUPPORTED
FTE Equivalent:	
Total Number:	

Student Metrics

This section only applies to graduating undergraduates supported by this agreement in this reporting period

The number of undergraduates funded by this agreement who graduated during this period: .....

The number of undergraduates funded by this agreement who graduated during this period with a degree in science, mathematics, engineering, or technology fields:.....

The number of undergraduates funded by your agreement who graduated during this period and will continue to pursue a graduate or Ph.D. degree in science, mathematics, engineering, or technology fields:.....

Number of graduating undergraduates who achieved a 3.5 GPA to 4.0 (4.0 max scale): .....

Number of graduating undergraduates funded by a DoD funded Center of Excellence grant for Education, Research and Engineering: .....

The number of undergraduates funded by your agreement who graduated during this period and intend to work for the Department of Defense .....

The number of undergraduates funded by your agreement who graduated during this period and will receive scholarships or fellowships for further studies in science, mathematics, engineering or technology fields: .....

Names of Personnel receiving masters degrees

NAME
Total Number:

Names of personnel receiving PHDs

NAME
Gilles Benoit
Fabien Sorin
Ofer Shapira
Shandon D. Hart
Total Number: 4

Names of other research staff

NAME	PERCENT_SUPPORTED
FTE Equivalent:	
Total Number:	

Sub Contractors (DD882)

Inventions (DD882)

Agile Photonic Crystals

Final Report

Yoel Fink

***Abstract*—We present an approach to the fabrication of functional fiber-based devices by thermal drawing in the viscous state termed the *preform-to-fiber* approach. A macroscopic preform rod containing metallic, semiconducting, and insulating constituents in a variety of geometries and close contact produces kilometer-long novel nanostructured fibers and fiber devices. A material identification scheme and the challenges of composite material processing are reviewed, and several devices and applications are discussed in detail. Metal-semiconductor-metal photosensitive and thermally-sensitive fibers are described. These flexible, light-weight, and low-cost functional fibers may pave the way for new types of fiber sensor devices, such as thermal sensing fabrics, artificial skins, and large-area optoelectronic screens. Next, the preform-to-fiber approach is used to fabricate spectrally tunable photodetectors that integrate a photosensitive core and a nanostructured photonic crystal defect cavity. An integrated self-monitoring optical transmission waveguide is then described that incorporates optical transport and thermal monitoring. The ability to predict power transmission failure is of paramount importance if high power optical transmission lines are to be operated safely and reliably in medical, industrial and defense applications. A hybrid electron-photon fiber consisting of hollow core (for optical transport by means of a photonic band gap) and metallic wires (for electron transport) is fabricated and may be used for transporting atoms and molecules by radiation pressure. Finally, a solid microstructured fiber fabricated with a highly nonlinear chalcogenide enables the generation of supercontinuum light at near-infrared wavelengths.**

I. Introduction

THE combination of insulating, semiconducting, and metallic elements in well-defined geometries and prescribed sizes, while forming intimate interfaces, is essential to the realization of practically all functional electronic, optoelectronic, and thermal devices [Chu95]. These devices are typically produced using a variety of elaborate wafer-based processes, which afford small features, but are restricted to planar geometries and limited coverage area. The use of this fabrication approach has been the cornerstone of the electronic revolution, but has had no impact on the optical fiber industry, which relies on a very different fabrication approach. Our goal here is to produce fibers that deliver electronic, optoelectronic, and thermal functionalities maintained over extended lengths of a fiber. Our strategy in achieving this goal is to use the preform-based fiber-drawing technique, which we call the *preform-to-fiber* approach, that has proven to be simple, and yet to yield extended lengths of highly uniform fiber with well controlled geometries and excellent optical and thermal properties [Har02, Tem02, Bay04Na, Bay04OP, Kur04, Bay05NM, Abo05, Bay05AM, Bay-Abo05]. The preform-to-fiber fabrication approach that we adopt thus relies on first preparing a large-scale macroscopic version of the required device in the form of a preform and then reducing it to the desired size through the process of thermal drawing. This process obviously places constraints on the materials that may be utilized. Nevertheless, a set of materials with widely disparate electrical, optical, and thermal properties has been identified and successfully incorporated into fiber-based devices.

In this report we discuss breakthroughs on four distinct fibers and fiber-based devices in detail. In the first design, illustrated in Fig. 1a, the photoconductive glass core contacted with metallic electrodes is surrounded with a multilayer resonant structure for external reflection. Such an arrangement allows for spectral manipulation of the externally incident light before reaching the metal-semiconductor-metal (MSM) photodetecting core [Bay04Na, Bay04OP, Abo05]. In the second design, depicted in Fig. 1b, a hollow-core photonic bandgap (PBG) transmission line is surrounded with a thin temperature-sensitive semiconducting glass layer contacted with electrodes, to form independent heat-sensing devices. In this structure, the heat escaping from the core into the cladding, when high-power laser beam coupled, is detected by means of electrical current when it reaches the thin-film layer [Bay05NM,Bay05AM]. In the

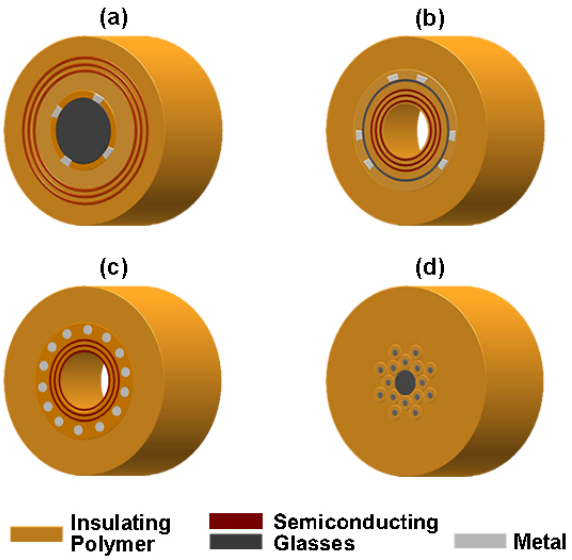

Fig. 1. (color) The *preform-to-fiber* approach yields novel fibers and functional fiber-based devices. (a) A spectrally tunable fiber photodetector having a photoconductive glass-core is surrounded by an externally reflecting resonant PBG structure. (b) An integrated self-heat-monitoring hollow-core PBG fiber which transmits a high-power laser beam while monitoring temperature inside the fiber by metal-semiconductor-metal thin-film heat sensors. (c) A dual electron-photon fiber transmits light through a hollow-core surrounded by mirror structure and electrical signal via metallic microwires along the length of the fiber. (d) Nonlinear, all-solid, nanostructured chalcogenide glass/polymer solid fibers for supercontinuum light generation.

third design, shown in Fig. 1c, an omnidirectional multilayer structure is surrounded with metallic electrodes, which allows simultaneous transport of electrons and photons along the fiber [Bay04Na]. In the last design, illustrated in Fig. 1d, the solid nanostructured fiber consists of a chalcogenide glass core and two-dimensional photonic crystal cladding. This fiber structure generates supercontinuum light at desired wavelengths when the highly nonlinear core is pumped with a laser [Bay-Abo05].

II. The Preform-to-Fiber Fabrication Approach

The process of optical-fiber drawing from a solid structured preform that is heated and deformed in the viscous state has been well established through the development of the fiber telecommunications industry, and enables the rapid fabrication of kilometer-scale continuous lengths of fiber with precise dimensional tolerances. The emerging field of microstructured silica [Rus03,Kni03, Egg01] and polymer [Eij01] optical fibers may be comprised of a single material combined with air holes relies on the controlled fabrication of sub-micron features.

However, our strategy is to produce multi-material composite fibers and fiber-based devices having optical, electrical, and thermal functionalities at nanometer feature sizes at kilometer length scales. This goal necessitates innovative fabrication approaches that allows for the use of new materials and geometries that have not been, hitherto, associated with fibers. By combining materials and exploring novel geometries, conventional functionalities can be enhanced and new ones introduced. This vision presents a unique set of challenges. Whatever the processing method, materials with potentially quite different electronic or optical properties must be compatible in such a way that enables the production of kilometers of fiber with submicron feature sizes, an aspect ratio on the order of 10^{10}.

Our core strategy is to use the familiar technique of thermal drawing a macroscopic fiber preform in the viscous state. This technique guarantees the production of kilometers of fibers at low cost and high uniformity. Several constraints, however, are imposed by the very nature of this technique, specifically in the choice of materials that are amenable to this type of processing. In particular, we discuss the use of a materials system that combines chalcogenide glasses, organic polymers, and metallic alloys in a macroscopic preform rod.

A. Material Selection

The main requirements in the materials used in these fibers are summarized as follows [Har04]:

- In general, materials should be glassy in order to be drawn at reasonable speeds in the fiber drawing process with self-maintaining structural regularity. Thus, our materials (or, at the very least, the majority component) must not simply be amorphous when deposited or made into a preform, but must remain amorphous and not crystallize when cycled through softening and drawing temperatures.

- The selected materials should exhibit low optical absorption over a common wavelength band. The penetration depth through multilayer structure is smaller than the absorption length.
- The materials must be above their respective softening points at overlapping temperatures to enable fiber co-drawing.
- The materials should have compatible viscosities at the processing temperatures of interest.
- The materials should exhibit good adhesion/wetting in the viscous and solid states without cracking even when subjected to thermal quenching.
- The metals and alloys should be molten at the drawing temperature during the fiber drawing process. Even though molten metals have very small viscosities, the capillary drawing confines the molten metals between semiconducting and insulating interfaces.

Various high-refractive-index chalcogenide glasses, low-refractive-index high-temperature thermoplastics, and low-melting-point metals and alloys are identified as potential candidates based on their optical and electrical properties, overlapping thermal softening regimes, and their amenability to film processing. Chalcogenides [Pop] are high-index inorganic glasses that contain two or more of the chalcogen elements (arsenic, sulfur, selenium, tellurium, germanium, tin, and gallium). These glasses have been explored due to their unique optical properties such as high nonlinearity [Harb02], wide transparency window at near- and mid-infrared wavelengths (up to 25 μm or higher), and high refractive indices (between 2.2 and 3.6). In particular, As-based chalcogenide glasses have low softening temperatures (between 100 and 300°C), high refractive index, and infrared transparency. Due to these unique properties, these glasses become an important class of materials in multilayer PBG fiber manufacture [Har02, Tem02, Kur04].

In selecting a low refractive index (n=1.3-1.7) component as the second material for these PBG fibers, it is of principal concern to match the thermal properties of some of the chalcogenide glasses. Thermoplastic polymers tend to have lower softening temperatures than typical chalcogenide glasses; however, a few candidates have been identified with thermal properties that are comparable to chalcogenides. Disadvantages of polymeric materials that may need to be addressed include their thermal stability and optical absorption. Nevertheless, the wide variety of polymers available, the feasibility of processing them in film form, and their excellent mechanical toughness make these materials our principal candidates for combination with chalcogenide glasses in composite PBG fibers [Har04]. In general, we used three different polymers, namely Polyethersulfone (PES), Polyetherimide (PEI), and Polysulfone (PS). Table I shows the thermal and optical properties of some of the chalcogenide glasses and polymers.

TABLE I
THERMAL AND OPTICAL PROPERTIES OF GLASSES AND POLYMERS

Materials	T_g (°C)	n (at 1.5 μm) n_0-ik	n (at 10.6 μm)	Transparency Window (μm)
As_2S_3	190	2.40	2.34	0.6-11
As_2Se_3	185	2.77	2.71	0.8-15
$Ge_{15}As_{25}Se_{15}Te_{45}$	190	3.32		1.5-16
PES	220	1.62-i0.0001	1.65-i0.0047	0 3-2.1[a,b]
PEI	215	1.65-i0.0017	1.66-i0.048	0.3-2.1[a,b]
PS	190	1.63		0 3-2.1[a,b]

The refractive indices were measured by using a Sopra GES5 UV-Vis-IR spectroscopic ellipsometer [Gil04].
[a] The transmittance is 90% or higher for 50-μm thick film.
[b] The k values are relatively low (transmittance is 65% or higher for 50-μm thick film) between 2.1-6.0, 9.3-11.3, and 12.2-13.6 μm.

Many metals, alloys, as well as eutectics, can be incorporated with the above polymers and chalcogenide glasses; for instance, Sn (T_M=232 °C), Bi (T_M=271 °C), In (T_M=157 °C), Sn(96%)-Ag(4%) (T_M=221-229 °C), and Pb(38%)-Sn(62%) (T_M=183 °C). Depending on the drawing temperature, we choose a suitable candidate from the above list.

B. Material Sythesis

The amorphous semiconductor glasses, As-Se [Kin95], As-Se-Te-Sn [Bay04Na], and Ge-As-Se-Te [Ina87,Ngu00, Tik04] are prepared from high purity Ge, As, Se, Te, and Sn elements using conventional sealed-ampoule melt-quenching techniques. The materials were weighed and placed into a quartz tube under a nitrogen atmosphere. The tube was heated to 330 °C for an hour at a rate of 1 °C/min under vacuum to remove surface oxides, and cooled to room temperature at the same rate. The ampoule was formed by sealing the tube under vacuum (~10^{-5} Torr). Depending on the actual composition, it was then heated to 800 °C (for As_2Se_3 and $As_{40}Se_{50}Te_{10}Sn_5$) or 900 °C (for $Ge_{15}As_{25}Se_{15}Te_{45}$) at a rate of 2 °C/min in a rocking furnace, while held vertical, for 24 hours and then rocked for 12 hours to increase mixing and homogenization. The glass liquid was cooled to 600 °C (700 °C for GAST) in the furnace, and then quenched in (cold for GAST) water. Subsequently, it was annealed for half an hour near the glass transition temperature before being cooled gradually to room temperature. As_2Se_3 glass used in supercontinuum generation was further purified by distillation. Using this procedure, mechanically stable glass rods with diameter ranging 5-18 mm and length 10-18 cm were obtained.

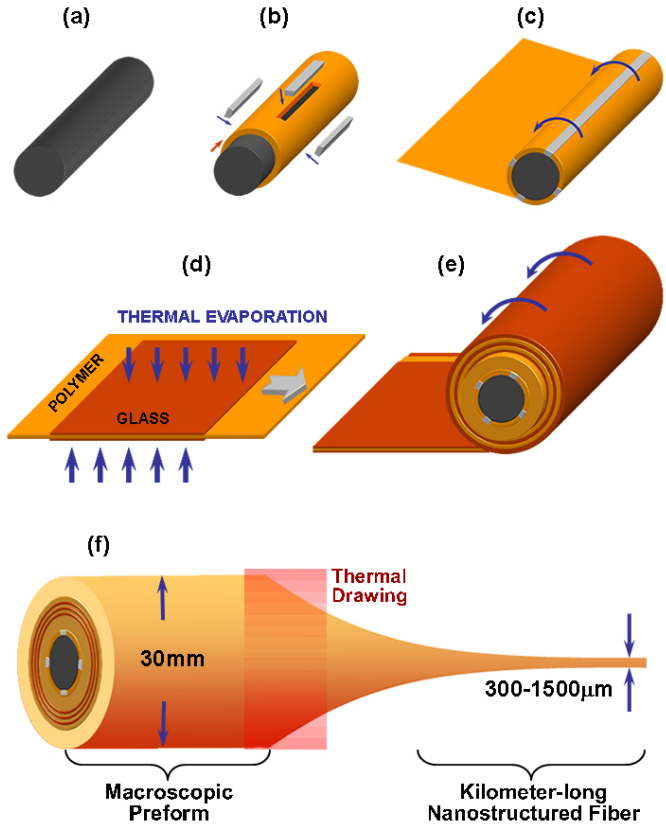

Fig. 2. (color) Fabrication steps for nanostructured fibers and fiber devices. (a) An amorphous glass is synthesized from elements in evacuated quartz tube. (b) The glass rod is assembled with an insulating polymer shell and four metal electrodes. (c) A polymer sheet is rolled around the structure to confine the metal conduits inside polymer. (d) A high-refractive-index glass is thermally evaporated on both sides of meters-long thin polymer film uniformly. (e) The evaporated film is rolled around the structure obtained in part (c). The final structure is then thermally consolidated in a vacuum oven in order to get a solid preform rod. (f) The preform is thermally drawn to kilometer-long mesoscopic-scale fibers containing micro- and nano-structures.

Commercially available polymer films are purchased from several suppliers: 25, 50, 75, and 125 μm thick PES from Westlake Inc (USA); 8, 10, 13, and 25 μm thick PEI from Nagai (Japan); and 25, 50, and 75 μm thick PS from Ajedium (USA).

C. Fabrication Procedure

We now discuss the fabrication of a structured preform essentially consisting of a semiconductor core (a chalcogenide glass), metallic electrodes (tin), and multiple alternating thin films (omnidirectional PBG structure) that are uniform and in intimate contact with each other. Even though the fabrication procedure varies for different structures proposed in Fig. 1, we explain the approach on the spectrally tunable fiber photodetecting device (Fig. 1a). A schematic outline of the steps involved in fabricating the preform is shown in Fig. 2:

- A semiconductor rod synthesized from elemental batch components in an evacuated quartz ampoule at 700-900 ^{o}C in a rocking furnace [Kin95] (Fig. 2a).
- A polymer tube obtained from thin film by rolling on a Teflon rod after consolidation in a vacuum oven. Four slits were opened, and the metallic electrodes placed these openings (Fig. 2b). Several layers of polymer film were rolled in order to confine the metallic electrodes (Fig. 2c).
- The thin-film deposition technique that we settled on was a thermal evaporation of the chalcogenide glass onto free-standing, commercially-obtained polymer films, allowing us to deposit layers of the chalcogenide glass at high deposition rates (Fig. 2d). We deposited uniformly 1.5-15 μm thick chalcogenide glasses on both sides of meters-long, 20-cm wide, and 8-50 μm thick polymer films.
- After rolling several polymer cladding layers, the preform was consolidated in a zone-defined horizontal vacuum oven while rotating the preform (Fig. 2e).
- The preform was then thermally drawn into hundreds of meters of fibers in a three-zone vertical tube furnace (Fig.

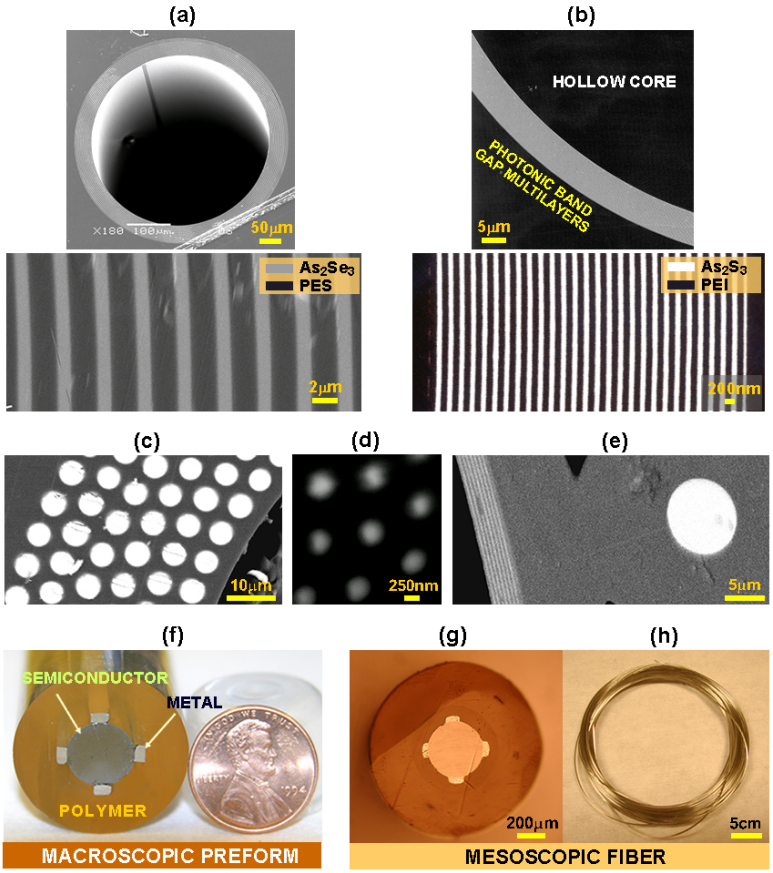

Fig. 3 (color). Examples of fibers and fiber devices produced by using the preform-to-fiber technique. Hollow-core, all-dielectric omnidirectional PBG fibers to guide laser light at (a) 10.6-μm and (b) 1.06-μm wavelengths. (c) Hexagonal PBG structure in fiber. A high-refractive-index glass (bright region) is embedded in a low-index polymer matrix. (d) Kilometer-long amorphous semiconducting nano-wires in a polymeric fiber. (e) Integration of optical (PBG multilayer mirror, left) and electrical (Sn micro-wire, right) elements in a fiber. (f-h) Fiber-based metal-semiconductor-metal light or heat sensors. Successful thermal drawing of a multi-material preform yields functional mesoscopic devices (g) in large length scale (h).

2f). The position of the PBG was measured by a Fourier transform infrared (FTIR) spectrometer (Bruker, Tensor 37) during the drawing process.

D. Examples

One class of fibers we produced using the above-mentioned technique are wavelength scaleable hollow-core omnidirectional PBG fibers. Figure 3a shows the scanning electron microscope (SEM) micrograph of a fiber having 11 cylindrical bi-layers of alternating As_2Se_3 and PES with thicknesses 1.07 and 1.96 μm, respectively. This fiber has a fundamental bandgap centered at 10.6 μm wavelength, which was designed to transport a high-power CO_2 laser beam. At the preform level, 13-μm thick As_2Se_3 film was uniformly deposited on both sides of a 45-μm thick, 22-cm wide, and 1-m long PES polymer film, and then rolled onto a teflon tube. The initial geometry and layer thickness ratio can be preserved during the fiber drawing process if suitable drawing conditions were chosen. Since the position of the bandgap of a multilayer mirror scales with layer thickness, one can obtain PBG guidance at shorter wavelengths by reducing the fiber's outer diameter. As shown in Fig. 3b, the fiber can transport Nd-YAG laser light centered around 1.05 μm with As_2Se_3 and PEI layer thicknesses of 101 and 160 nm, respectively.

The second class of fibers contain two-dimensional photonic crystal structures (Fig. 3c-d). The high-index glass-core (bright regions) fibers with polymer cladding were used to construct a preform, and then drawn into microstructured fibers. After several consecutive drawings, it is possible to reach a reduction factor (initial preform feature size/final fiber feature size) order of $5x10^5$. The SEM micrograph of kilometer long semiconducting nanowires with diameter around 200 nm in a polymer matrix is shown in Fig. 3d. We expect that one can to reach an ultimate length scale less than 20 nm in such a material system [Har04].

The third class of structures integrates optical and electrical elements on the same fiber. As shown in Fig. 3e, a

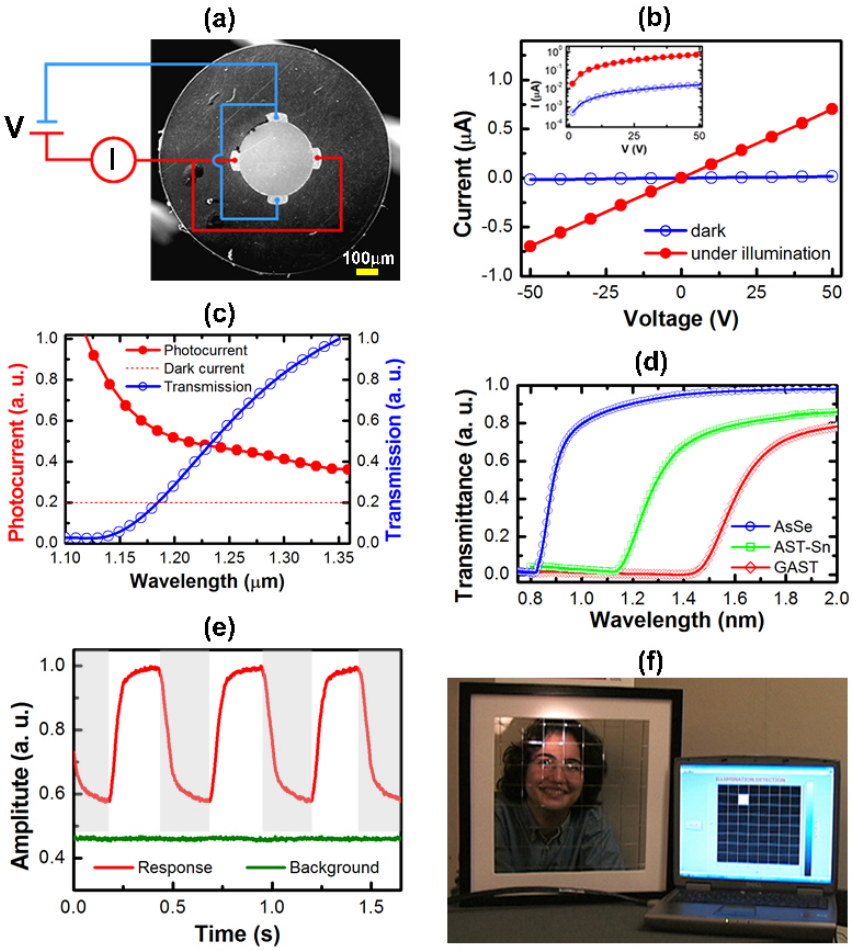

Fig. 4. (color) The metal-semiconductor-metal (MSM) fiber photodetectors. (a) SEM micrograph of the entire cross-section of a MSM device. The device is connected to external circuitry through four metallic electrodes running along the fiber length. (b) Current-voltage characteristics of the MSM fiber photodetector in the dark and under illumination. (c) Measured photocurrent sweeping wavelength of tunable OPO while keeping the optical power constant and transmission spectrum of bulk Sn-doped AST chalcogenide glass. (d) Tunability of operation wavelength by changing glass composition. (e) Temporal response of the fiber device. (f) A 2D fiber web can be used to track a point of illumination in real time.

cylindrical multilayer optical mirror combines with a micron scale wire which is running along the fiber length. The fourth class is integrated fiber-based functional devices containing metallic, semiconducting, and insulating elements in a variety of geometries. Figure 3f shows a macroscopic preform rod a MSM fiber device which sense light or heat depending on the semiconductor core. The fiber device (Fig. 3g) is connected to the external circuitry through metallic electrodes running along meters-long fiber (Fig. 3f). Optical or thermal excitation on any point along the fiber device generates electrical current.

III. Metal-Semiconductor-Metal Fiber Photodetectors

Light detection on curved surfaces and large areas is a task that has yet to be achieved in a convenient way. We present a new methodology for light detection on large areas by using flexible, low-cost, light-weight, mechanically tough, and arbitrarily long one-dimensional photodetectors [Bay04Na, Bay04Op, Aym05]. Underlying this approach is a new fiber structure that senses impinging light along its entire length and generates an electrical signal.

The photodetecting fibers were obtained from a macroscopic preform (33-mm thick and 20-cm long) consisting of a cylindrical semiconductor chalcogenide glass core ($As_{40}Se_{50}Te_{10}Sn_5$, AST-Sn), contacted by four Sn metal conduits that are encapsulated in a protective PES cladding. This highly photoconductive AST-Sn glass is optimized subject to the following requirements: (1) large photoconductivity in the spectral range of interest, (2) the viscosity range should be compatible with the polymer, and (3) an enhanced stability against crystallization during fiber drawing. The preform was consolidated in a three-zone horizontal tube furnace at 260 ^{o}C under vacuum (10^{-3} Torr) while rotating the preform along its axis, and was subsequently heated and drawn into hundreds of meters of fiber. The preform geometry was

preserved throughout all thermal processes, i.e., consolidation and drawing. The fiber exhibits both electrical and optical functionalities that follow from the excellent contact and appropriate element dimensions. Figure 4a shows the cross-section of a 980-μm-thick fiber which is connected to an external circuit though the metallic electrodes. The electrical conductance of this fiber was found to increase dramatically upon illumination by white light (by two orders of magnitude for 20 mW incident power, see Fig. 4b). The current-voltage (I-V) curve reveals clear ohmic response both in the dark and under illumination.

Next we characterized the broad-band photoconductive response of the device fiber (the red curve in Fig. 4c). The fiber was illuminated externally with a laser beam from a tunable, synchronously pumped optical parametric oscillator (Mira OPO, Coherent). The optical transmission of a bulk AST-Sn glass sample (12-mm diameter and 5-mm length) was obtained via an FTIR measurement (blue curve in Fig. 4c). A 50-volt DC voltage was applied to the fiber and the current was measured using a pico-ampere meter (Yokogawa/Hewlett Packard 4140B). The spectral photoconductive response is commensurate with the optical transmission measurement. Note that changing the chemical composition of the glass core can change the spectral characteristics of the photoconductive response, as seen in Fig. 4d where the optical transmission spectra corresponding to As_2Se_3, $As_{40}Se_{50}Te_{10}Sn_5$ and $Ge_{15}As_{25}Se_{15}Te_{45}$ are plotted. The onset of optical transmission, and hence the drop in the photoconductivity, is shifted by changing the glass composition. Indeed, the photoconductive glass in the core may be substituted with other families of glasses that are sensitive to other physical quantities, such as temperature [Bay05AM] or chemical contaminants. An example of the temporal response of the MSM device fiber is depicted in Fig. 4e.

While the individual fiber behaves as a one-dimensional photodetector with sensitivity to visible and infrared light at every point along its entire length, it is the assembly of such fibers into 2D grids or photodetector fiber webs that enables the detection of an illumination point. Moreover this grid achieves N^2 detection resolution with only $2N$ elements. An example of such a fiber web used to measure the coordinates of an illumination point on a 30x30 cm^2 area consisting of 64 resolved points is shown in Fig. 4f. The web is made of 16 fibers arranged in an 8×8 grid. When light is incident on any of the fibers, a photocurrent is generated, and the voltage on the fiber changes. Each fiber is connected to an operational amplifier (in unity-gain configuration) that matches its impedance to that of a data acquisition card placed in a PC. A computer program monitors the voltages supplied (16 in total), which indicate the amount of light incident on each fiber. The program identifies the voltages related to the horizontal and vertical fibers, and then identifies the location of the light beam. When no light is incident on the grid, the voltage drops on the fibers assume their 'dark' values, and the 'virtual grid' on the computer screen is uniformly black. The horizontal (vertical) fiber that undergoes the maximum change in voltage determines the vertical (horizontal) coordinate of the incident beam. A white spot is then placed on the virtual grid at the location of the horizontal and vertical coordinates thus determined. The voltage on the fibers are monitored continuously, and the refresh rate is limited by the relaxation time of the fibers and the speed of the data acquisition card.

IV. Spectrometric Photodetecting Fibers

One may integrate a PBG resonant structure with a photodetecting fiber to produce a narrow-band tunable fiber photodetector (Fig. 1a). The PBG structure contains an optical cavity and is introduced in the optical path shielding the photoconducting core from ambient illumination sources. Upon external illumination, when the wavelength of the radiation matches that of the cavity resonance, one observes an electric response from the fiber core thus establishing the spectroscopic functionality of the fiber [Bay04Na].

The preform of this spectroscopic fiber consists of a photoconductive chalcogenide glass rod ($As_{40}Se_{50}Te_{10}Sn_5$), having diameter 12 mm and length 18 cm, contacted by four Sn conduits, and surrounded by a quarter-wave As_2Se_3/PEI multilayer mirror structure with a λ/2 PEI cavity and a protective PES cladding. The preform was consolidated in a three-zone horizontal tube furnace at 260 ^oC under vacuum (10^{-3} Torr) while rotating the preform along its axis. Subsequently, the preform was drawn in a three-zone vertical tube furnace at a top zone temperature between 185 and 230 ^oC and a middle zone temperature 295 ^oC. A capstan speed of about 0.7-3 m/min produced a fiber of a diameter between about 1200 μm and 500 μm, and a length of several hundred meters. Figure 5a shows SEM micrographs of the spectroscopic fiber cross section. The resonant PBG structure encapsulating the MSM photodetecting devices is shown in Fig. 5b. For a 920-μm-thick fiber, the thicknesses of As_2Se_3 and PEI layers are 117 and 204 nm, respectively. The photograph in Fig. 5c is a spectrometric mesh-grid weaved from fibers having different outer diameters; each strand in the mesh-grid can detect a specific wavelength that matches the resonance frequency of its Fabry-Perot structure.

The resonance wavelength and PBG is determined by the device fiber outer diameter. From the fabricated fibers of various diameter we selected (and, therefore, a wide range of resonant wavelengths) three fibers of outer diameters 870, 890, and 920 μm. The reflectivity of the optical-cavity structure was measured for fibers having these diameters with an

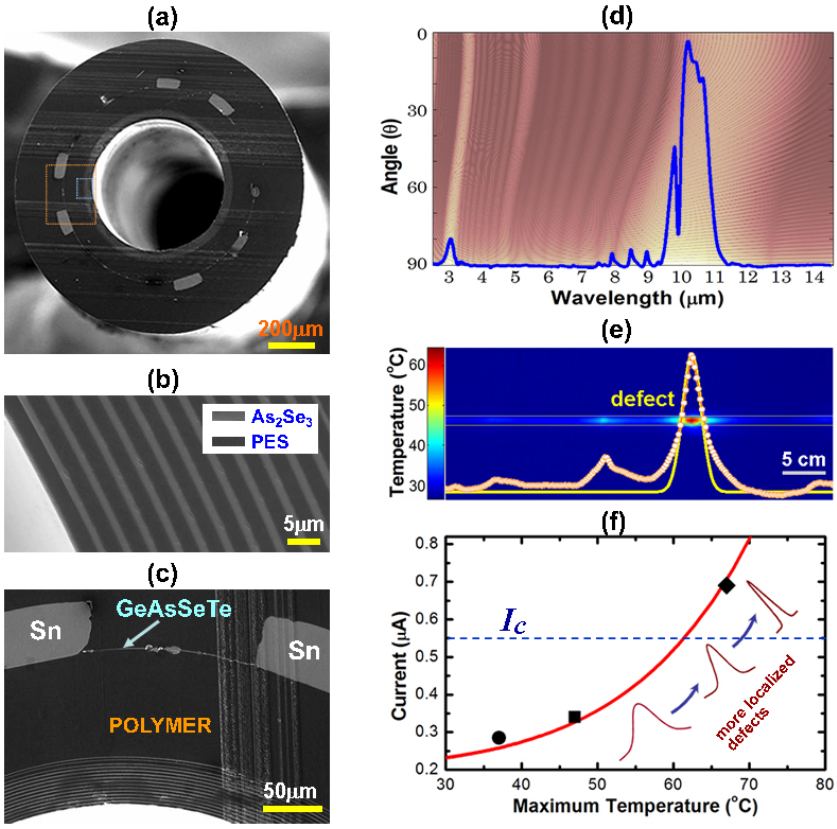

Fig. 6. (color) An integrated self-heat-monitoring fiber. SEM micrographs of the integrated fiber; (a) the entire cross section, (b) the cylindrical omnidirectional Bragg mirror, and (c) the metal-semiconductor-metal (MSM) heat sensor. (d) Calculated band diagram of cylindrical multilayer PBG structure and corresponding measured broad-band transmission spectrum (solid line). (e) Thermal photograph of a fiber containing a single localized defect, along with the measured (circles) and fitted (solid line) temperature distribution along the fiber. (f) Calculated current as a function of the maximum temperature along the fiber for a constant dissipated power (solid line) and three experimental points.

Fig 200 mag diff laser beam. (f) Simultaneously measured photocurrents through the device fibers.

FTIR spectrometer (Nicolet/SpectraTech, NicPlan infrared microscope and FTIR [Magna 860]) and are displayed in Fig. 5d. The FTIR spectra agree well with the calculated spectra when averaging over the range of angles admitted by the microscope objective (0 to 35°, numerical aperture of 0.58) is taken into consideration, leading to a reduction in the apparent quality factor of the cavity mode [Gil05]. The primary band gap of the mirror structure extends from 1 to 1.6 microns. The visible colors in Fig. 5c are due to second order reflections from the surface of the fibers.

In order to characterize the optoelectronic response of our integrated device fiber, it is useful to measure both the electrical photocurrent and the optical reflectivity simultaneously. This can be achieved by externally illuminating the three aforementioned fibers with a laser beam and measuring the back-reflected light though a beam splitter, while simultaneously monitoring the generated photocurrent in the photosensitive core. For optical characterization, we used a Verdi10 (Coherent) to pump a Ti-S femtosecond laser (Mira 900, Coherent) that was then down-converted using a synchronously pumped OPO (Mira OPO, Coherent). The OPO beam was focused onto the outer surface of the fiber using a ×5 microscope objective (NA=0.1), and the back-reflected light from the fiber was directed through a beam splitter to an InGaAs photodetector (Newport 818-IG). The optical power incident on the fiber surface was maintained at 30 mW using a variable optical attenuator, while the wavelength of the laser beam was swept. For simultaneous electrical characterization, we measured the current flowing through the fiber electrodes using a pico-ampere meter (Yokogawa/Hewlett Packard 4140B). The DC voltage difference applied to the two fiber electrodes was 50 volts. At each wavelength, the incident optical power was adjusted, the electrical current was recorded, and the back-reflected light power measured.

In Fig. 5e, we displayed the measurement results of the back-reflected light from these fibers as the wavelength of a laser beam (from the tunable OPO) is swept. Concurrently, we plotted the results of photocurrent measurements of

these fibers (Fig. 5f). At the resonance wavelength, the back-reflection is diminished, and the light reaches the photoconductive core. Consequently, the corresponding photocurrent is enhanced. This integrated optoelectronic fiber device functions as a narrowband photodetector, with the detected wavelength tuned through the fiber outer diameter.

V. Self-Heat-Monitoring Integrated Fibers for High-Power Laser Beam Delivery

The ability to integrate optical transport and thermal monitoring for failure prediction is of paramount importance if high-power optical transmission lines [Abe04, Kat02, Day05] are to be operated safely and reliably in medical, industrial and defense applications [Har]. Recently, the use of hollow-core PBG fibers for in-vivo endoscopic surgery on human patients and canine larynges has been successfully demonstrated [Dev05]. However, fibers used for laser surgery transport significant laser power through their core and even a small defect nucleating within such a high power optical transmission line can result in unintentional energy release with potentially detrimental or catastrophic consequences.

We designed and fabricated a fiber device structure (Fig. 6a) which contains integrated optical, electrical and thermal elements for self monitored optical transport [Bay05NM]. This multi-material fiber comprised of a polymer insulator (PES), a binary large bandgap semiconductor (As_2Se_3), a quaternary narrow bandgap semiconductor ($Ge_{15}As_{25}Se_{15}Te_{45}$ (GAST)), and metallic elements (Sn) is drawn at high speeds from a single fiber preform to produce extended lengths of optically and thermally functional fibers. An optical transmission element which is a hollow-core multilayer (Fig. 6b) cylindrical PBG structure [Fin98] designed to guide high-power radiation at 10.6 microns along the fiber axis [Tem02]. Multiple thermal-detection elements, (Fig. 6c) are placed in the vicinity of the hollow-core for the purpose of temperature monitoring along the entire fiber length. Metal wires bridged by a temperature-sensitive semiconductor layer extend along the length of the fiber and deliver an electrical response to the fiber ends upon change in the fiber temperature.

The macroscopic preform rod, which shares the final fiber geometry, was prepared by the following steps:

- A 13-μm thick film of As_2Se_3 was thermally evaporated on both sided of a 50-μm thick, 24-cm wide, and 40-cm long PES film, that was then rolled onto a 14.2-mm thick teflon FEP rod which does not stick to the inner glass layer during thermal processing steps.
- The 10-μm thick GAST film was then deposited by thermal evaporation with a vacuum evaporator (Ladd Industries) on one side of a 50-μm thick PES film. After rolling a few-millimeters-thick buffer PES layer, the single GAST layer was rolled.
- This temperature-sensitive GAST layer was contacted by six Sn (tin) metal conduits (0.8 mm thick, 2.5-mm wide, and 15-cm long) that are encapsulated in a protective PES cladding.
- The preform was consolidated for 70 minutes at 260 ^{o}C under vacuum (~10^{-3} Torr) in a three-zone horizontal tube furnace, and the teflon rod was removed from the core after consolidation. The preform was annealed and then cooled gradually to room temperature.

The preform was subsequently heated and drawn into tens of meters of fiber in a draw tower (Heathway). Fibers were drawn at the central zone of a three-zone vertical tube furnace (Thermcraft) with the top-zone temperature 190 ^{o}C and the middle-zone temperature 295 ^{o}C. The fiber diameter was monitored with laser diameter monitors and the target fiber diameter was determined by measuring broad-band FTIR spectra during drawing.

We first discuss the optical transport properties of this hybrid fiber. The fiber has a 1270-μm-thick outer diameter and a 560-μm-diameter hollow core surrounded by a multilayer structure consisting of 13 bilayers of alternating As_2Se_3 and PES having thicknesses of 1 μm and 1.9 μm, respectively (see Fig. 6b). The calculated PBG diagram of the hybrid fiber is depicted in Fig. 6d, revealing an omnidirectional bandgap extending from 9.4 to 11.4 μm. The light gray areas represent guided modes inside the core, while dark gray areas correspond to regions where light is not guided, but instead radiates through the multilayer structure. The transmission spectrum of a 1-m long fiber was measured by the FTIR spectrometer and is overlaid on the band diagram in Fig. 6d.

To demonstrate the delivery of high-power laser light through the hybrid fiber while monitoring the temperature in the fiber, a CO_2 laser (GEM-25, Coherent-DEOS) at 10.6 μm was coupled to the fiber and a 50-V DC voltage was applied to the device electrodes. The input and output optical power as well as the current through the electrodes were recorded. We measured the power radiated from the fiber outer surface and also obtained thermal images using an infrared (IR) camera (FLIR). The power escaping from the surface of the fiber was found to be negligible with respect to the overall power loss, suggesting that the difference in power between the input and output dissipates in the fiber cladding and converts into heat.

In order to investigate the self-fault-detection capabilities of our fiber, we measured the current as a function of the dissipated power for three 40-cm long fibers: (1) a defect-free, (2) a bent defect-free, and (3) a single-defect-containing fiber. The defect on the fiber was intentionally generated by burning a small spot on the fiber with a CO_2 laser beam.

The temperature distribution along the single-defect-containing fiber is shown in Fig. 6e. While indeed power is dissipated throughout the entire fiber length, it is the localized defect site that undergoes the most significant heating (Fig. 6e). This heating, in turn, causes an exponential increase in the semiconductor's conductivity, which results in an increase in the current flow (Fig. 6f). The three experimental points shown in Fig. 6f correspond to a defect-free straight fiber (circle), a bent fiber (square), and a single-defect-containing straight fiber (diamond). The current exceeds a threshold value, I_c, only for the defect case. Thus, the exponential dependence on temperature of the electrical conductivity of the semiconducting material allows for the discrimination - in real time - between normal transmission conditions and those which are indicative of localized defect formation, enabling for the first time a self monitoring high power optical transmission line for failure prediction and prevention.

Incorporating a thermal element with optical structures may potentially yield various optoelectronic devices such as fiber-based tunable mid-infrared attenuators and thermo-optic switches [Bay05UP]. We expect that flexible, thin, low-cost, large-area, distributed, mechanically tough, and polymeric fiber-based heat sensors might be used in medical, military, industrial, and space applications [Bay05AM].

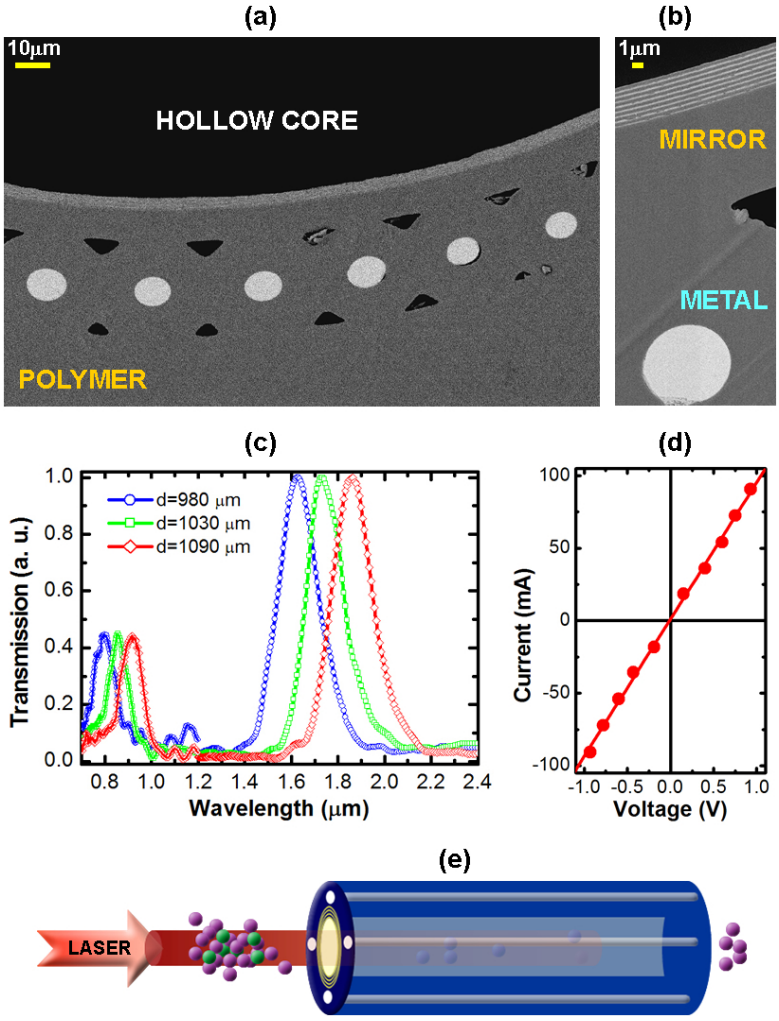

Fig. 7. (color) Dual electron-photon transport fiber. (a) SEM micrograph of the cross section of the hybrid fiber with 800-μm hollow core, omnidirectional mirror layers, metallic filament array, and polymer cladding. (b) Magnified SEM micrograph of 8 pairs of quarter wave dielectric As_2Se_3/PEI multilayers with sub-micron feature sizes and a metallic micro-wire. (c) Measured transmission spectra of three fibers having different outer diameters exhibiting PBG guidance through air core. The primary and second order photonic band gaps are located at 1.62 μm and 0.8 μm for the 980-μm thick fiber, and are shifted to longer wavelengths as the fiber diameter increases. (d) Measured electrical current along the 980-μm thick fiber, 15-cm long, as a function of applied bias voltage. (e) Schematics of laser-assisted atom or particle guiding through hollow-core hybrid fibers.

VI. Hybrid Electron-Photon Transport Fibers

Conventional optical fibers guide light in a solid core via total internal reflection. This process has fundamental limitations stemming from light absorption by electrons and phonons, material dispersion, Rayleigh scattering, thermal lensing, end-point reflections, and optical nonlinearities. These limitations have motivated the study of light propagation through hollow-core in metallic [Abe94, Kat02], dielectric [Mar64], micro-structured silica [Kni03] and polymer [Eij01], and Bragg waveguides [Yar78, Fin98, Har02]. Hollow-core fibers promise high-energy laser delivery [Har04, Tem02], atom or particle guiding [Ren95, Ben02], chemical and biological molecules sensing [Cha05], and high-harmonic generation [Run98]. Having electrical transmission lines in close contact to optical counterpart is critical for certain applications [Lar03]. To date, incorporation of optical and electrical functionalities in micron-scale fibers has not been achieved. We present the design and fabrication of a new hybrid fiber structure that allows us to transmit electrons and photons simultaneously [Bay04NA].

The macroscopic preform of hybrid fiber was assembled by wrapping a PEI film (8-μm thick, 20-cm wide, and 1-m long), coated on both sides with a 2.6-μm thick layer of As_2Se_3, around a pyrex tube having 16-mm outer diameter. An array of Sn strands were positioned around the outer surface of the multilayer structure by using a polymer solution of 20% PES, 80% N,N-dimethylacetamide. The resulting preform was then consolidated in a vertical rotating furnace at a

temperature of 260°C and a pressure of 10^{-3} Torr. The preform longitudinal axis is held vertically in the furnace and a zone-refining heating process is carried out along the preform length. After consolidation, the preform was immersed in a liquid HF bath for 3 hours to selectively etch away the pyrex tube in the center, leaving a hollow core. The finalized preform was then drawn under the following conditions: a temperature of 302°C, a downfeed speed of 0.003 mm/sec, and a capstan speed of 1 m/min. The metal-core polymer-cladded fiber strands used in the preform were obtained by drawing a preform with 5-mm Sn (99.75% purity) core and 7.5-mm PES cladding. The preform was consolidated in a vacuum oven at 260° C, and then drawn at ~305° C in a vertical tube furnace. Both ends of the preform were sealed with polymer to confine the metal during the consolidation and drawing processes. Meters of metallic fibers with outer diameters from 500 μm to 1.2 mm were successfully drawn and sectioned into strands.

The dual electron-photon fiber, shown in Fig. 7a, is comprised of a hollow core, surrounded by a multilayer dielectric mirror [Fin98, Kur04] formed from 8 pairs of alternating layers of As_2Se_3 and PEI (layer thicknesses of 150 and 280 nm, respectively). This multilayer structure provides the optical confinement to the low-index core. Immediately adjacent to this omnidirectional mirror is a circular array of 60 Sn metal strands with diameters of ~8 μm each. The whole fiber is then surrounded with a PES polymer cladding.

The optical transport characteristics of the fiber are determined by the positions of the photonic bandgaps. For example, fibers having outer diameters of 980, 1030, and 1090 μm have fundamental bandgaps centered at 1.62, 1.75, and 1.85 μm, and second order band gaps around 0.80, 0.85, and 0.92 μm, respectively (see Fig. 7c). Optical transmission spectra were determined using an FTIR spectrometer (Bruker Tensor 37). In order to examine the electrical properties of the fiber, on the other hand, both ends of the fiber were coated with a thick layer of gold that electrically connects all the Sn wires. The current-voltage characteristics of the 980-μm thick fiber are displayed in Fig. 7d, showing clear ohmic response.

We have performed a systematic investigation of the losses incurred upon propagation through simple (non metal containing) hollow-core multilayer photonic bandgap fibers in Refs. [Tem02, Kur04]. The loss of such fibers for radiation at a wavelength of 10.6 μm was found to be less than 1 dB/m [Tem02]. More recently, we have characterized such fibers at a wavelength of 1.5 μm, and measured losses to be 2.0dB/m [Kur04, Jeff05]. The loss mechanisms are found to be (1) radiation through the multilayers, (2) intrinsic material absorption, (3) nonuniformity in the layer thicknesses, and (4) scattering due to internal surface roughness. Since light is strongly confined within the hollow core by the cylindrical omnidirectional mirror, it is expected that the presence of additional material components or structural complexity lying outside of the cylindrical mirror will not significantly affect the losses through this hollow fiber. Indeed, initial loss measurements on the electron-photon transport fibers yield loss levels that are comparable to the cylindrical photonic bandgap fibers of similar structural characteristics.

There has been widespread interest in guiding cold atoms, particles, and bacteria in hollow-core optical fibers via radiation pressure [Ash87, Ren95, Ben02] or magnetic quadrupole [Key00]. We expect that the hybrid PBG optical fibers can improve mesoscale particle guidance in miniature transmission lines in many respects (see Fig. 7e): (1) Strong omnidirectional confinement yields much longer transport length due to low loss. (2) Flexibility of polymeric fibers and low-bending loss can enhance guiding efficiency through sharp corners. (3) Generating an electric field by applying potential differences on electrodes allows the separation of charged particles from neutral ones. (4) Generating a quadrupole at the center of fiber can further confine particles in very small region.

VII. Spectral Broadening in Microstructured Solid Glass/Polymer Fibers

Spectral broadening of laser pulses via self-phase-modulation (SPM) [Sto78] in single-mode chalcogenide optical fibers has recently attracted much attention for supercontinuum generation [Fu05,Slu04,Gop04]. Since chalcogenide glasses have high a nonlinear index (n_2) compared to silica (2-3 orders of magnitude depending on composition), one may obtain significant spectral broadening in very short fibers or even waveguides on a chip. Here we report on a new microstructured, all-solid, glass/polymer fibers, and investigated the optical and nonlinear properties of these fibers [Bay-Abo05OE].

The small-core fibers were fabricated as follows: (1) 10-mm thick As_2Se_3 rod was synthesized as explained in Sec. II. (2) A 25-mm thick cylindrical preform was obtained by rolling 75-μm thick PES film onto the rod. (3) The preform was consolidated in a vacuum oven, and subsequently drawn into 750-μm thick fibers. (4) Some of these fibers were cut into 20-cm long pieces, and placed around 9-mm thick As_2Se_3 rod in order to construct 4 rings. (5) After rolling some PES as a protective cladding; 23-mm thick preform was consolidated and drawn into fibers. (6) A 20-cm long and 830-μm thick fiber was placed inside of a previously drawn hollow PES fiber (core and outer diameters are around 830 μm and 3.1 mm, respectively). (7) A 33-mm thick preform was obtained by rolling some PES film onto this thick PES fiber, and then consolidated; subsequently drawn into fibers having diameters between 400 μm and 900 μm. Figure 8a

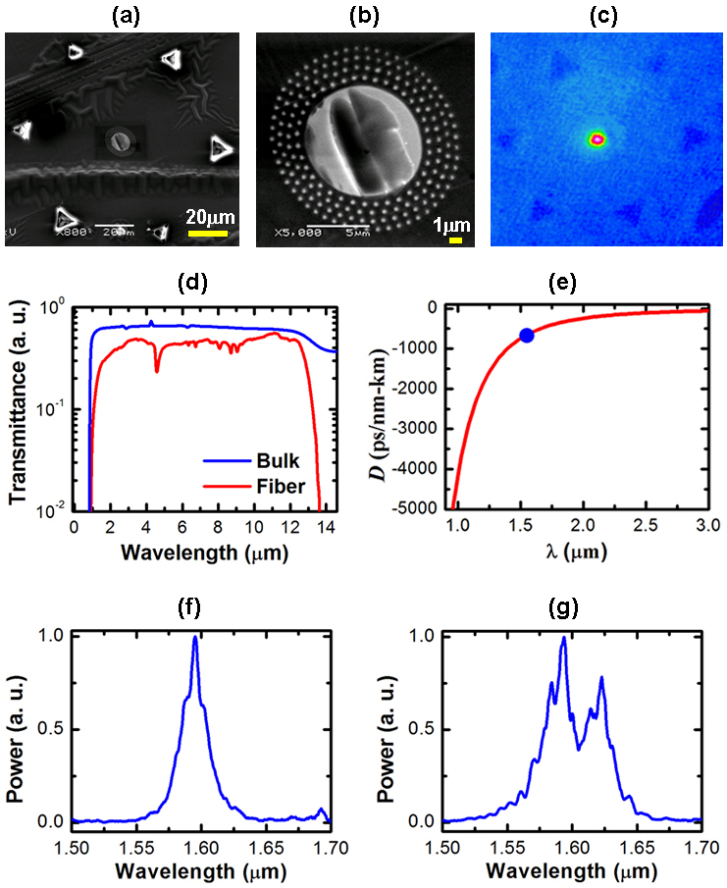

Fig. 8. (color) Nonlinear, microstructured, all-solid, small-core chalcogenide/polymer fiber. (a) SEM micrograph of the cross-section of a small-core fiber. (b) Magnified SEM shows 9-μm glass core (As_2Se_3), 4 rings of glass/polymer nano-structured cladding. (c) Microscope image of light coming out from small-core fiber at 1.6 μm wavelength. (d) Broad-band FTIR transmission spectrum for a bulk glass disk and a large-core (300-μm) fiber. (e) Material dispersion for bulk As_2Se_3 glass obtained from ellipsometric measurements. (f) Output spectra for 1.7 mW average input power. (g) The spectral broadening at 56 mW input power.

shows SEM micrograph of an 880-μm thick fiber having 9-μm thick As_2Se_3 core surrounded by 4 nanostructured rings (Fig. 8b). A laser beam at 1.6 μm wavelength was coupled to a 15-cm long fiber, and the output beam profile measured by using a high-resolution detector (Sensor Unlimited). As shown in Fig. 8c, the output beam profile is gaussian and single mode.

The broad-band transmission spectra of a bulk sample (9-mm in diameter and 3-mm thick) and a large-core fiber (10-cm long and 300-μm thick core) were measured by using an FTIR (Bruker, Tensor 37). Both sides of the disk and fiber were polished by using 10, 3, 1, and 0.3 micron aluminum oxide films (South Bay Technology) in order to get optical surfaces. As shown in Fig. 8d, the bulk As_2Se_3 glass has a wide transparency window starting 0.8 microns up to 16 microns while large-core fiber transmits light between 0.9 and 13.5 microns. The absorption related to H-Se (λ=4.25 μm) impurities can be removed after further distillation [Ngu02].

The refractive index of the bulk As_2Se_3 glass was measured by using a spectroscopic ellipsometer (Sopra GES5 UV-Vis-IR), and fitted to the Cauchy formula: $n(\lambda)=A+B/\lambda^2+C/\lambda^4$, with parameters A=2.7391, B=0.0599, and C=0.0443. The material dispersion was determined from $D=-\lambda/c\ d^2n/d\lambda^2$, where c is the speed of light. As shown in Fig. 8e, the dispersion is negative and large around the telecommunications wavelength, and gets smaller for longer wavelengths. We estimated D = -552 ps/nm-km at 1.55 μm, which is very close the value reported in Ref. [Slu05].

In order to demonstrate the spectral broadening via SPM in our small-core microstructured fibers, we coupled an OPO laser (Mira, Coherent) beam by using a x20 microscope objective to 3-cm long and 6.3-μm core fiber. The output light was collected with x100 microscope objective and sent to an optical spectrum analyzer (Ando) via a multi-mode silica fiber. While the spectrum is identical with input spectrum for low power (1.7 mW), there is a significant spectral broadening at high powers. We observed a spectrum broadening about 150% for 56 mW input power compared to the input spectrum (Fig. 8g). Modification of the nanostructure around the solid core allows tailoring the total dispersion.

VIII. Conclusion

We have shown that the repertoire of structures and devices that may be produced by the familiar thermal drawing of macroscopic preforms in the viscous state is not limited to the materials or structures to which this approach has been confined. We have shown that materials having disparate optical and electrical properties, including metals, semiconductors, and insulators may be incorporated into this process with careful material selection and processing. The fiber devices we have produced demonstrate intimate contacts between the different materials that enable novel functionalities to be realized at optical-fiber length and cost. Nano-scale ordered photonic structures may also be produced with this perform-to-fiber approach, and more than one structure may be integrated into the same fiber device. It is safe to expect that many more devices and functionalities, enabled by exploring more materials and geometries, will be realized through this approach.

References

[1] S. L. Chuang, "Physics of optoelectronic devices," John Wiley, 1995.

[2] S. D. Hart, G. R. Maskaly, B. Temelkuran, P. H. Prideaux, J. D. Joannopoulos, and Y. Fink, "External Reflection from omnidirectional dielectric mirror fibers," *Science*, vol. 296, pp. 510-513, Apr. 2002.

[3] B. Temelkuran, S. D. Hart, Wavelength-scalable hollow optical fibres with large photonic bandgaps for CO_2 laser transmission, *Nature*, vol. 420, pp. 650-653, Dec. 2002.

[4] M. Bayindir, F. Sorin, A. F. Abouraddy, J. Viens, S. D. Hart, J. D. Joannopoulos, and Y. Fink, "Metal–insulator–semiconductor optoelectronic fibres," *Nature*, vol. 431, pp. 826-829, Oct. 2004.

[5] M. Bayindir, A. F. Abouraddy, F. Sorin, J. D. Joannopoulos, and Y. Fink, "Fiber photodetectors codrawn from conducting, semiconducting, and insulating materials," *Opt. and Photon. News*, vol. 15, pp. 24, Dec. 2004.

[6] K. Kuriki, O. Shapira, S. D. Hart, G. Benoit, Y. Kuriki, J. F. Viens, M. Bayindir, J. D. Joannopoulos, and Y. Fink, "Hollow multilayer photonic bandgap fibers for NIR applications," *Opt. Express*, vol. 12, pp. 1510-1517, Apr. 2004.

[7] M. Bayindir, O. Shapira, D. Saygin-Hinczewski, J. Viens, A. F. Abouraddy, J. D. Joannopoulos, and Y. Fink, "Integrated fibres for self-monitored optical transport," *Nature Materials*, vol. 4, pp. 820-825, Nov. 2005.

[8] M. Bayindir, A. F. Abouraddy, J. D. Joannopoulos, and Y. Fink "Thermal-sensing mesoscopic fiber devices by composite-material processing, Submitted," *Advanced Materials*, 2005.

[9] A. F. Abouraddy, O. Shapira, M. Bayindir, J. Arnold, F. Sorin, D. S. Hinczewski, J. D. Joannopoulos, and Y. Fink, "Large-area optical-field measurements with geometric fibre constructs," Submitted (2005).

[10] M. Bayindir, A. F. Abouraddy, J. D. Joannopoulos, and Y. Fink "Supercontinuum generation in solid chalcogenide glass/polymer fibers," In preparation, 2005.

[11] J. A. Harrington, *Infrared Fibers and Their Applications.* SPIE Press, 2004.

[12] A. K Devaiah, S. M. Shapshay, U. Desai, G. Shapira, O. Weisberg, D. S. Torres, and Z. Wang, "Surgical utility of a new carbon dioxide laser fiber: Functional and histological study," *Laryngoscope*, vol. 115, pp. 1463-1468, Aug. 2005.

[13] Y. Fink, J. N. Winn, S. Fan, C. Chen, J. Michel, J. D. Joannopoulos, and E. L. Thomas, "A dielectric omnidirectional reflector," *Science*, vol. 282, pp. 1679-1682, Nov. 1998.

[14] M. A. Popescu, *Non-Crystalline chalcogenides*. Kluwer, Dortrecht 2000, pp. 115.

[15] V. Q. Nguyen, J. S. Sanghera, F. H. Kung, P. C. Pureza, and I. D. Aggarwal, "Very large temperature-induced absorptive loss in high Te-containing chalcogenide fibers," *J. Lightwave technol.*, vol. 18, pp.1395-1401, Oct. 2000.

[16] V. K. Tikhomirov, D. Furniss, A. B. Seddon, J. A. Savage, P. D. Mason, D. A. Orchard, K. L. Lewis, "Glass formation in the Te-enriched part of the quaternary Ge–As–Se–Te system and its implication for mid-infrared optical fibres," *Infrared Phys. Technol.*, vol. 45, pp. 115-123, Mar. 2004.

[17] I. Inagawa, R. Iizuka, T. Yamagishi, and R. Yokota, "Optical and thermal properties of chalcogenide Ge-As-Se-Te glasses for IR fibers," *J. Non-Cryst. Solids*, vol. 95-96**,** pp. 801-808, Dec. 1987.

[18] T. Abel, J. Hirsch, and J. A. Harrington, "Hollow glass waveguides for broadband infrared transmission," *Opt. Lett.*, vol. 19, pp. 1034-1036, July 1994.

[19] T. Katagiri, Y. Matsuura, and M. Miyagi, "Metal-covered photonic bandgap multilayer for infrared hollow waveguides," *Appl. Opt.*, vol. 41, pp. 7603-7606, Dec. 2002.

[20] A. Dayan, A. Goren, and I. Gannot, "Theoretical and experimental investigation of the thermal effects within body cavities during transendoscopical CO_2 laser-based surgery," *Laser Surg. Med.*, vol. 35, pp. 18-27, July 2004.

[21] G. Benoit, http://mit-pbg.mit.edu/Pages/Ellipsometry.html

[22] A. Ashkin and J. M. Dziedzic, "Optical trapping and manipulation of viruses and bacteria," *Science*, vol. 235, pp. 1517-1520, Mar. 1987.

[23] M. J. Renn, D. Montgomery, O. Vdovin, D. Z. Anderson, C. E. Wieman, and E. A. Cornell, "Laser-guided atoms in hollow-core optical fibers," *Phys. Rev. Lett.*, vol. 75, pp. 3253-3256, Oct. 1995.

[24] F. Benabid, J. C. Knight, and P. S. J. Russell, "Particle levitation and guidance in hollow-core photonic crystal fiber," *Opt. Express*, vol. 10, pp. 1195-1203, Oct. 2002.

[25] M. Key, I. G. Hughes, W. Rooijakkers, B. E. Sauer, E. A. Hinds, D. J. Richardson, and P. G. Kazansky, "Propagation of cold atoms along a miniature magnetic guide," *Phys. Rev. Lett.*, vol. 84, pp. 1371-1373, Feb. 2000.

[26] L. B. Fu, M. Rochette, V. G. Ta'eed, D. J. Moss, and B. J. Eggleton,"Investigation of self-phase modulation based optical regeneration in single mode As_2Se_3 chalcogenide glass fiber," *Opt. Express*, vol. 13, pp. 7637-7644 , Jan. 2005.

[27] R. E. Slusher, G. Lenz, J. Hodelin, J. Sanghera, L. B. Shaw, and I. D. Aggarwal, "Large Raman gain and nonlinear phase shifts in high-purity As_2Se_3 chalcogenide fibers," *J. Opt. Soc. Am. B*, vol. 21, pp. 1146-1155, Jun. 2004.

[28] J. M. Harbold, F. Ilday, F. W. Wise, J. S. Sanghera, V. Q. Nguyen, L. B. Shaw, and I. D. Aggarwal, "Highly nonlinear As-S-Se glasses for all-optical switching," *Opt. Lett.*, vol. 27, pp. 119-121, Jan. 2002.

[29] T. Gopinath, H. M. Shen, H. Sotobayashi, E. P. Ippen, T. Hasegawa, T. Nagashima, and N. Sugimoto, “Highly nonlinear bismuth-oxide fiber for smooth supercontinuum generation at 1.5 µm,” *Opt. Express*, vol. 12, pp. 5697-5702, Nov. 2004.
[30] R. H. Stolen and C. Lin, “Self-phase-modulation in silica optical fibers,” *Phys. Rev. A*, vol. 17, pp. 1448-1453, Apr. 1978.
[31] B. J. Eggleton, C. Kerbage, P. Westbrook, R. S. Windeler, and A. Hale, “Microstructured optical fiber devices,” *Opt. Express*, vol. 9, pp. 698-713, Dec. 2001.
[32] M. van Eijkelenborg, M. Large, A. Argyros, J. Zagari, S. Manos, N. A. Issa, I. M. Bassett, S. C. Fleming, R. C. McPhedran, C. M. de Sterke, and N. A. P. Nicorovici, “Microstructured polymer optical fibre,” *Opt. Express*, vol. 9, pp. 319-327, Sep. 2001.
[33] E. A. J. Marcatili and R. A. Schmeltzer, “Hollow metallic and dielectric wave-guides for long distance optical transmission and lasers,” *Bell Syst. Tech. J.*, pp. 1783-1809, Jul 1964.
[34] P. Yeh, A. Yariv, and E. Marom, “Theory of Bragg fiber,” *J. Opt. Soc. Am.*, vol. 68, pp. 1196-1201, Sep. 1978.
[35] S. D. Hart, PhD Thesis, Massachusetts Institute of Technology, 2004.
[36] A. Rundquist, C. G. Durfee, Z. Chang, C. Herne, S. Backus, M. M. Murnane, and H. C. Kapteyn, “Phase-matched generation of coherent soft x-rays,” *Science*, vol. 280, pp 1412-1415, May 1998.
[37] C. Charlton, B. Temelkuran, G. Dellemann, and B. Mizaikoff, “Midinfrared sensors meet nanotechnology: Trace gas sensing with quantum cascade lasers inside photonic band-gap hollow waveguides,” *Appl. Phys. Lett.*, vol. 86, no 194102, May 2005.
[38] M. Bayindir, J. D. Joannopoulos, and Y. Fink “Fiber-based tunable attenuators for infrared wavelengths” *Unpublished*, 2005.
[39] V. Q. Nguyen, J. S. Sanghera, P. C. Pureza, F. H. Kung, and I. D. Aggarwal, “Fabrication of arsenic selenide optical fiber with low hydrogen impurities,” *J. Am. Ceram. Soc.*, vol. 85, pp. 2849-2851, Nov. 2002.
[40] W. A. King, A. G. Clare, and W. C. Lacourse, “Laboratory preparation of highly pure As_2Se_3 glass,” *J. Non-Cryst. Solids*, vol. 181, pp. 231-237, Feb. 1995.
[41] M. Large, A. Argyros, G. Barton, I. Bassett, F. Cox, M. Fellew, G. Henry, N. Issa, S. Manos, W. Padden, L. Poladian, M. A van Eijkelenborg, and J. Zagari, “Microstructured optical fibers: Why use polymers?” *Proc. 29th Eur. Conf. on Opt. Comm. (ECOC’03 Rimini)*, pp. 1014-1017, 2003.
[42] P. Russell, “Photonic crystal fibers,” *Science*, vol. 299, pp. 358-362, Jan. 2003.
[43] J. C. Knight, “Photonic crystal fibres,” *Nature*, vol. 424, pp. 847-851, Aug. 2003.
[44] M. van Eijkelenborg, M. Large, A. Argyros, J. Zagari, S. Manos, N. A. Issa, I. M. Bassett, S. C. Fleming, R. C. McPhedran, C. M. de Sterke, and N. A. P. Nicorovici, "Microstructured polymer optical fibre," *Opt. Express*, vol. 9, pp. 319-327, Sep. 2001.
[45] G. Benoit, K. Kuriki, J. F. Viens, J. D. Joannopoulos, and Y. Fink, “Dynamic all-optical tuning of transverse resonant cavity modes in photonic bandgap fibers,” *Opt. Lett*, vol. 30, pp. 1620-1622, Jul. 2004.